Available online at www.sciencedirect.com
SCIENCE DIRECT®
Physica A 343 (2004) 201–218
PHYSICA A
www.elsevier.com/locate/physa

Spatial correlations and synchronization in coupled map lattices with long-range interactions

D.B. Vasconcelos[a], R.L. Viana[a,*], S.R. Lopes[a], A.M. Batista[b], S.E. de S. Pinto[b]

[a]*Departamento de Física, Universidade Federal do Paraná, 81531-990 Curitiba, Paraná, Brazil*
[b]*Departamento de Matemática e Estatística, Universidade Estadual de Ponta Grossa, 84033-240 Ponta Grossa, Paraná, Brazil*

Received 19 February 2004; received in revised form 3 May 2004
Available online 14 July 2004

Abstract

We used numerical diagnostics to quantify spatial disorder, and its relation with temporal chaos, for a one-dimensional chain of coupled logistic maps with a coupling strength which varies with the lattice distance in a power-law fashion. The main tool is spatial return plots, whose properties are used to obtain information about the chaotic synchronized states of the system. A spatial correlation integral is introduced to characterize the clustering of points in the spatial return plots.

PACS: 05.45.Ra; 05.45.Jn; 05.45.Xt

Keywords: Coupled map lattices; Synchronization; Spatial correlations

1. Introduction

Partial differential equations form the backbone of mathematical physics, and their solution techniques, analytical as well as numerical ones, are present in the

*Corresponding author.
E-mail address: viana@fisica.ufpr.br (R.L. Viana).

0378-4371/$ - see front matter
doi:10.1016/j.physa.2004.06.063

standard tool-box of any physicist. Nevertheless, other spatially extended dynamical systems have received much attention in the past decades as simplified models for a variety of spatio-temporal phenomena, yet retaining some of the essential features universally recognized in partial differential equations. Discretization of spatial variables in a regular or disordered lattice leads to oscillator chains, for which the evolution of the state variables attached to each lattice site is governed by ordinary differential equations. Spatial coupling between lattice sites leads to non-trivial behavior, a fact already recognized in the earliest computer investigations on such systems, as those performed by Fermi, Pasta, and Ulam in the 1950s [1].

The interplay between generation of local dynamics and diffusion of vector quantities along the lattice was already appreciated by Turing [2] in a landmark work on what is currently known as "reaction–diffusion systems", and which also influenced the ensuing work by the Brussels school of Prigogine and coworkers [3] on the theme. Further modeling simplification results from discretizing also the time variable, what can be accomplished, for example, if the local generation of dynamics in each lattice site occurs in an impulsive form. There results a lattice of coupled maps, for which both space and time are discretized, yet allowing a continuous state variable. Coupled map lattices become popular after the pioneering work of Kaneko and collaborators [4], and they are widely recognized as simple models which still share many dynamical properties with more complex systems.

One of the main motivations to investigate the dynamical properties of coupled map lattices has been the quest for understanding the onset of turbulence in fluids and plasmas, a problem which challenged theoretical physicists during many decades [5]. Unfortunately lattice coupled systems have severe limitations to model turbulent systems, in that they have a cutoff in the wave numbers which can be studied, due to the finite spatial resolution inherent to the lattice. Nevertheless, a close relative of turbulence, or *spatio-temporal chaos*, can be successfully studied with coupled map lattices [6]. Chaté and Manneville have shown that the transition to spatio-temporal chaos has analogous features with directed percolation, but with a different universality class [7].

By spatio-temporal chaos, roughly speaking, we mean a situation where the temporal dynamics is chaotic and the spatial distribution of map iterates is "random" or weakly correlated [8]. The characterization of chaotic time dynamics can be made, for example, through the Lyapunov spectra or the Kolmogorov–Sinai entropy of the coupled map lattice. On the other hand, the characterization of spatial randomness is still an open problem, with various methods proposed to accomplish this task, like gradient pattern analysis, which has proved useful to evidence spatio-temporal intermittency and localized turbulence [9]; and generalized complex entropic forms, which permits us to quantify the degree of phase disorder associated with a given gradient field [10]. Both methods have used coupled map lattices as theoretical laboratories for numerical analyses which can be further carried out in studies of turbulence in fluids and plasmas.

Most previous works on this subject have focused on coupled map lattices with local interactions, for which only the nearest-neighbor sites contribute to the lattice coupling [4]. This paper focuses on coupled map lattices for which the interaction

between sites is long-ranged, the coupling strength decreasing with the lattice distance in a power-law fashion. Non-local couplings such as this have been used to model neural network architectures with local production of information [11,12]; partial integro-differential equations modeling physico-chemical reactions [13]; assemblies of biological cells with oscillatory activity, and whose interaction is mediated by some rapidly diffusing chemical substance [14]; and systems of diffusion coupling in nucleation kinetics, with elimination of the rapidly diffusing components [15].

The power-law coupling to be considered in this paper presents an effective range parameter, in such a way that we are able to pass continuously from a local to a global coupling scheme. It was previously used for studies of an extended Kuramoto model [16], chains of coupled kicked limit-cycle oscillators [17], sine-circle map lattices [18], and van der Pol oscillators [19]. In this work we focus on the characterization of spatial randomness in coupled map lattices, by considering diagnostics which put into evidence spatial patterns ranging from complete disorder to synchronization. We make a kind of "attractor reconstruction" for the high-dimensional coupled map system, by obtaining a spatial return plot, which amounts to a low-dimensional embedding of the original system [20]. The distribution of the points on such return plots can give valuable information about coherent behavior like synchronization of periodic and chaotic dynamics [21]. In particular, we propose the use of a spatial analogue of the correlation integral [22] to investigate the dependence of spatial correlation caused by total or partial synchronization with the effective coupling range.

The rest of this paper is organized as follows: in Section 2 we present the coupled map lattice model to be used, and a preliminary discussion based on the decay of spatial correlations. Section 3 shows numerical analyses using spatial return maps, and a numerical characterization of the approach to the synchronized behavior. The spatial correlation integral is introduced in Section 4, with an analysis of its dependence with the effective coupling range. Our conclusions are left to the final section.

2. The coupled map lattice

As a representative example of coupled chaotic maps which has been extensively studied over the past years, we examine a one-dimensional lattice of N coupled logistic maps $x \mapsto f(x) = \mu x(1-x)$, where $\mu \in [0,4]$, and $x_n^{(i)} \in [0,1]$ represents the state variable for the site i ($i = 1,2,\ldots,N$) at time n. We use a non-local form of coupling for which the interaction strength decreases with the lattice distance in a power-law fashion, and whose normalized form is given by [17,23,24]

$$x_{n+1}^{(i)} = (1-\varepsilon) f(x_n^{(i)}) + \frac{\varepsilon}{\eta(\alpha)} \sum_{j=1}^{N'} \frac{1}{j^{\alpha}} \left[f(x_n^{(i+j)}) + f(x_n^{(i-j)}) \right], \tag{1}$$

where $\varepsilon > 0$ and $\alpha > 0$ and

$$\eta(\alpha) = 2 \sum_{j=1}^{N'} \frac{1}{j^{\alpha}} , \tag{2}$$

with $N' = (N-1)/2$, for N odd.

In the coupled map lattice given by Eq. (1), the summation term stands for a weighted average of discretized second spatial derivatives, the normalization factor $\eta(\alpha)$ being the sum of the corresponding weights. In the limit $\alpha \to \infty$, only the $j = 1$ term will survive in the summation term, resulting in $\eta \to 2$ and the Laplacian or diffusive coupling

$$x_{n+1}^{(i)} = (1-\varepsilon) f(x_n^{(i)}) + \frac{\varepsilon}{2} [f(x_n^{(i+1)}) + f(x_n^{(i-1)})] , \tag{3}$$

in which only the nearest-neighbors of a given site contribute to the coupling term [25–27]. The other limiting case, $\alpha = 0$, is such that $\eta = N - 1$ and the map lattice becomes globally coupled

$$x_{n+1}^{(i)} = (1-\varepsilon) f(x_n^{(i)}) + \frac{\varepsilon}{N-1} \sum_{j=1, j\neq i}^{N} f(x_n^{(j)}) , \tag{4}$$

where each map interacts with the mean value of all lattice sites, irrespective of their positions (“mean-field” model) [28]. Hence, the coupling term in Eq. (1) may be regarded as an interpolating form between these limiting cases.

Chaotic dynamics in a lattice with N coupled maps can be studied by means of its Lyapunov spectrum, consisting of N ordered exponents $\lambda_1 = \lambda_{max} > \lambda_2 > \cdots > \lambda_N$. It may well happen that many of such exponents are positive, hence a quantity of interest is the density of Kolmogorov–Sinai (KS) entropy

$$h = \langle \lambda_j \rangle_{j, \lambda_j > 0} = \frac{1}{N} \sum_{j=1}^{\lambda_j > 0} \lambda_j . \tag{5}$$

Actually, this expression, according to the Pesin’s theorem, gives only an upper bound on the density of KS-entropy [29,30].

Fig. 1 shows the dependence of the KS-entropy density with the coupling strength ε and effective range α, for a coupled logistic lattice of $N = 1001$ maps at outer crisis ($\mu = 4$), for which the uncoupled maps have Lyapunov exponent $\lambda_U = \ln 2$. We used periodic boundary conditions for the lattice ($x_n^{(i)} = x_n^{(i \pm N)}$) and random initial conditions $x_0^{(i)}$, $i = 1, 2, \ldots, N$. In the global coupling limit ($\alpha = 0$), it turns out that h is very small for strong coupling (large ε). This indicates that, if there is chaotic dynamics in the system, it is restricted to a very small number of degrees of freedom. As we will see in Section 4, in this case there is only one degree of freedom exhibiting chaos out of the N dimensions of the phase space of the coupled map lattice. This occurs because of a collective effect in that all coupled maps are synchronized in amplitude, even though their dynamics is chaotic. The single degree of freedom characterized by a positive Lyapunov exponent is related to a one-dimensional

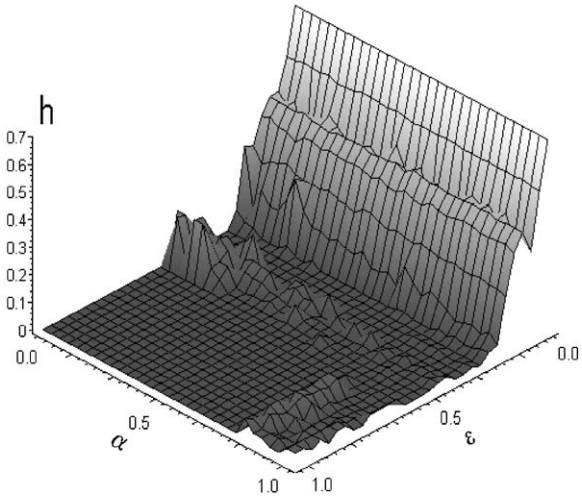

Fig. 1. Density of KS entropy of $N = 1001$ coupled logistic map lattice of form (1) versus coupling strength and range, using $a = 4$, periodic boundary conditions and random initial conditions.

manifold embedded in the phase space of the system. Approximately at $\varepsilon \approx 0.2$ the value of h starts to builds up monotonically until it reaches its maximum value λ_U in the case of zero coupling.

We still have such a transition for higher α, but the increase of the KS-entropy slows down and becomes oscillatory for strong coupling. When ε goes to zero, h eventually has the same steep and monotonic increase which we have seen in a global coupling. The coupling between maps becomes effectively noticeable with nearest-neighbors for large α, and even a strong coupling does not change the chaotic dynamics of each map, although the number of positive Lyapunov exponents diminishes as the coupling strength ε grows. A sudden decrease in the KS-entropy can be observed when both α and ε have larger values, which is a consequence of a chaos suppression mechanism by pattern selection. In fact, it has long been known that, for the so-called frozen random pattern, there is a decrease of the entropy with increase of non-linearity [26].

3. Spatio-temporal chaos and its characterization

Unlike the chaotic dynamics of the lattice, the characterization of spatio-temporal chaos is still an open problem in both analytical and numerical points of view. A rigorous definition of spatio-temporal chaos in coupled map lattices has been given by Bunimovich and Sinai, as follows [31]: let a d-dimensional lattice be represented by Z^d, and let $\mathsf{M} = \bigotimes_{i\in\mathsf{Z}^d} \mathsf{M}_i$ be the N-dimensional phase space of the coupled map lattice, consisting of the direct product of local phase spaces M_i, which are copies of the unit interval $[0, 1]$ (in the case of $f(x)$ being the logistic map).

The coupled map lattice is a time map Φ acting on this phase space, and preserving the lattice structure $\Phi(\mathbf{x}) = \{\Phi_i(\mathbf{x})\}_{i\in\mathsf{Z}^d}$, where $\Phi_i : \mathsf{M} \to \mathsf{M}_i$ is the restriction of the map Φ to site i. Let S be the shift operator on the lattice Z^d, hence the spatio-temporal dynamics in a coupled map lattice is generated by the temporal dynamics Φ and the spatial dynamics S. The system is said to exhibit spatio-temporal chaos if there exists an invariant measure μ, unique for any finite restriction of the lattice, such that the dynamical systems (M, μ, Φ) and $(\mathsf{M}, \mu, \mathsf{S})$ are both mixing [32].

The difficulty in rigorously proving that a given coupled map lattice exhibits spatio-temporal chaos lies in the finding of such a Sinai–Ruelle–Bowen (SRB) measure, which has the following important properties: (i) the measure is invariant under both space and time translations; (ii) the measure is smooth along unstable eigendirections in the phase space; (iii) the measure has strong ergodic properties, including mixing and positive KS-entropy [33]. SRB measures were obtained for certain classes of coupled expanding circle maps [31,33,34].

Since a rigorous characterization of spatio-temporal chaos is restricted to a few cases, it turns out that, for practical purposes, we identify its existence by means of two predicates: (i) decay of time correlations; (ii) decay of spatial correlations over the lattice. Note that this is not, strictly speaking, equivalent to spatio-temporal chaos, since these properties do not refer to the interplay between spatial and temporal degrees of freedom. Accordingly, we shall characterize spatial randomness by analyzing the properties of the lattice profiles at a fixed time.

Let us consider, for a fixed time n, the average value of the map amplitudes over the entire lattice: $\langle x\rangle_n = (1/N)\sum_{i=1}^{N} x_n^{(i)}$. The corresponding deviations from this average are $\hat{x}_n^{(i)} = x_n^{(i)} - \langle x\rangle_n$. The average quadratic deviation

$$\delta x_n \equiv \left[\frac{1}{N-1}\sum_{i=1}^{N}\left(\hat{x}_n^{(i)}\right)^2\right]^{1/2}, \tag{6}$$

can be used as a quantitative measure of roughness for a given spatial profile [35]. In this work, however, we deal with the spatial correlation function, defined as

$$E_n(\ell) \equiv \frac{(1/N)\sum_{i=1}^{N}\hat{x}_n^{(i)}\hat{x}_n^{(i+\ell)}}{(1/N)\sum_{i=1}^{N}(\hat{x}_n^{(i)})^2} \tag{7}$$

for a given time n and spatial displacement $\ell = 1, 2, \ldots$ (notice that, due to the periodic boundary conditions assumed, the spatial displacement is measured in a given ring).

Fig. 2(a) is an amplitude versus space pattern for a coupled map lattice of form (1) with $\varepsilon = 0.5$ and $\alpha = 2.0$ (i.e., an essentially local coupling, for which only nearest-neighbors are taken into account), and at a fixed time n. The spatial randomness is reflected by the fast decay of the spatial correlation function (Fig. 2(b)), computed for a given site of the coupled lattice. Previous analyses have pointed out that the decay of spatial correlations in coupled lattices of strongly chaotic maps presents a power-law decay [36].

If we change the coupled map lattice parameters such that the spatial randomness is somewhat reduced, for example lowering the α parameter such that the coupling

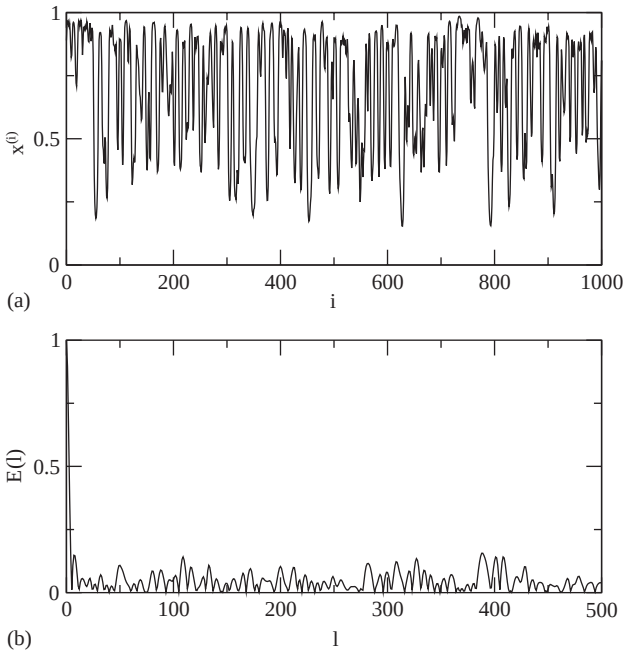

Fig. 2. (a) Spatial profile of the coupled map lattice (1) with $N = 1001$, $\mu = 4.0$, $\varepsilon = 0.5$ and $\alpha = 2.0$ at a fixed time $n = 5000$; (b) Spatial correlation function as a function of the lattice separation, for this profile.

becomes more of a global nature (Fig. 3(a)), the corresponding spatial correlation function would also decay, but in a slower fashion with respect to the spatial delay ℓ (Fig. 3(b)). Moreover, unlike the previous case, in which after a fast decay the correlation presents low-amplitude fluctuations, now the correlations grow up after a slower decay.

4. Spatial return plots and synchronization

In the early days of research on coupled map lattices, an important issue was the study of the transition from N-torus (quasi-periodic states) to chaos through the so-called spatial mode instabilities [37]. To evidence these behaviors, Kaneko has introduced the very useful notion of a spatial return plot [25]. In its simplest form, it is just a plot of each site amplitude (at a fixed time) $x_n^{(i)}$ *versus* the amplitude of its nearest neighbor $x_n^{(i+1)}$. It is a convenient way to visualize the tori appearing in spatially quasi-periodic states and their breakup *via* zig-zag structure formation, spatial mode instabilities, and soliton-like structure generation and propagation.

More generally, we can resort to the powerful embedding techniques of non-linear series analysis to borrow the idea of an spatial embedding. In this case the spatial delay can be taken as one site, but this restriction can be lifted whenever necessary.

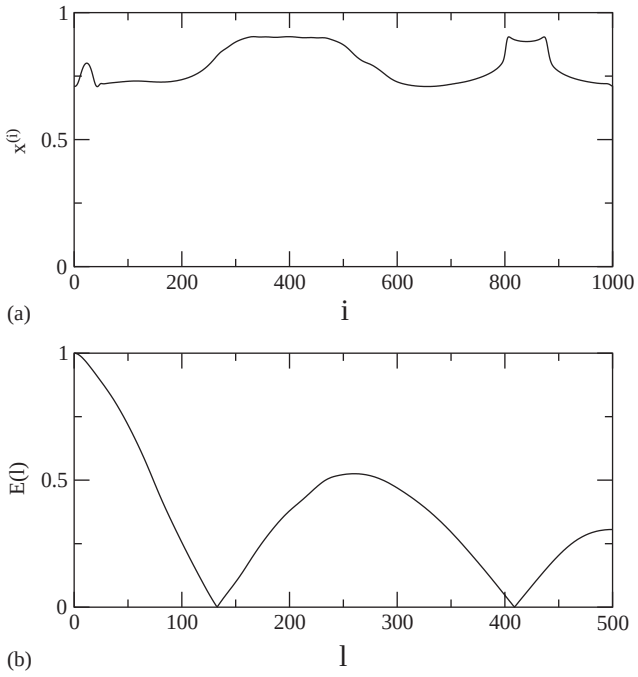

Fig. 3. (a) Spatial profile of the coupled map lattice (1) with $N = 1001$, $\mu = 4.0$, $\varepsilon = 0.5$ and $\alpha = 0.5$ at a fixed time $n = 5000$; (b) Spatial correlation function as a function of the lattice separation, for this profile.

Given a spatial pattern for a fixed time n, $\{x_n^{(1)}, x_n^{(2)}, \ldots, x_n^{(N)}, x_n^{(N+1)} = x_n^{(1)}\}$, we can form an immersion in a vector space of embedding dimension D, by choosing a vector with "delay coordinates":

$$\xi_n^{(i)} \equiv (x_n^{(i)}, x_n^{(i+1)}, \ldots, x_n^{(i+\mathsf{D}-1)}) \,. \tag{8}$$

In Figs. 4(a)–(f) we plot a sequence of $D = 2$-dimensional spatial return plot for a lattice of $N = 1001$ logistic maps and a fixed time. We considered six combinations involving weak and moderately strong coupling, as well an effective range parameter varying from global to local interactions. By virtue of our construction, there is an approximate symmetry of the plots with respect to the diagonal line $\mathscr{S} : x_n^{(i+1)} = x_n^{(i)}$.

When there is no spatial correlation at all between the coupled maps, even though their dynamics is periodic, we expect the return plot to consist of a cloud of scattered points, what can be seen in Figs. 4(a)–(c), for weak coupling (small ε). As the coupling prescription becomes global (decreasing α) the overall behavior does not change much, except that the cloud appears to concentrate in a sub-interval of $[0, \sqrt{2}]$ along $\mathscr{S}$. Increasing the coupling strength ε we see that, even for a local coupling (Fig. 4(d)) there is a visible concentration of points around the diagonal line, which augments for intermediate (Fig. 4(e)) and global (Fig. 4(f)) coupling.

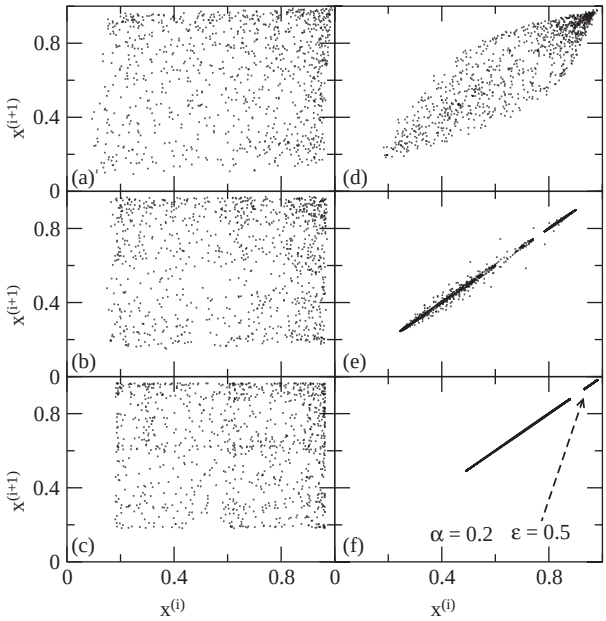

Fig. 4. Spatial return maps for a coupled map lattice (1) with $N = 1001$ and (a) $\alpha = 2.0$, $\varepsilon = 0.1$; (b) $\alpha = 1.0$, $\varepsilon = 0.1$; (c) $\alpha = 0.5$, $\varepsilon = 0.1$; (d) $\alpha = 2.0$, $\varepsilon = 0.5$; (e) $\alpha = 1.0$, $\varepsilon = 0.5$; (f) $\alpha = 0.5$, $\varepsilon = 0.5$ (large plot) and $\alpha = 0.2$, $\varepsilon = 0.5$ (small plot).

If the maps were completely synchronized at a same value $x_n^{(i)} = \chi$ for a given time (this can occur both for periodic and chaotic time dynamics, as n evolves), the spatial return map would consist of just one point along the diagonal line. This nearly occurs when the coupling range is near to the mean-field case, as can be seen in the small diagonal dash at the lower left-hand side of Fig. 4(f), representing a case where $\alpha = 0.2$.

Hence, we can give a quantitative measure of how far a spatial pattern is from being completely synchronized, at a given time n, by computing the orthogonal distance

$$d_n^{(i)} \equiv \frac{1}{\sqrt{2}} (x_n^{(i)} - x^{(i+1)}) \tag{9}$$

of each point in the (two-dimensional) spatial return map from the diagonal line $\mathscr{S}$. The normalization factor $1/\sqrt{2}$ stems from the coordinate change one performs when rotating by 45° the axes in order to make one of them coincide with the diagonal line. Due to the approximate symmetry of the plot with respect to the diagonal line, it turns out that the average value of $d_n^{(i)}$ is nearly zero. Hence, a better choice would be to compute the average absolute value $\bar{d}_n = (1/N) \sum_{j=1}^{N} |d_n^{(j)}|$ or the corresponding mean quadratic deviation, with similar results.

In the next section, it will be useful to work also with the orthogonal distance, in the whole N-dimensional phase space of the coupled map lattice, between the phase point $(x_n^{(1)},\ldots,x_n^{(N)})$ and the synchronization manifold, defined by $x_n^{(1)}=x_n^{(2)}=\cdots=x_n^{(N)}$. It reads, for a fixed time n,

$$D_n^2=\sum_{j=1}^{N}(x_n^{(j)})^2-\left(\frac{\sum_{j=1}^{N}x_n^{(j)}}{\sqrt{N}}\right)^2. \tag{10}$$

We can also write this distance as $D_n^2=N\sigma_n^2$, where

$$\sigma_n^2=\langle x^2\rangle_n-\langle x\rangle_n^2 \tag{11}$$

is the variance of the map amplitudes with respect to their lattice average $\langle x\rangle$ at a given time n.

The sequence of Figs. 5(a)–(d) represents the average absolute value of the distance between the points in the spatial return plot to the diagonal line $\bar{d}_n$ versus the coupling strength and effective range parameter, at a fixed time $n=5000$. The various superimposed lines represent five different random initial conditions for the lattice. Basically for all of them there is a clear trend to decrease the average distance $\bar{d}_n$ as the coupling becomes stronger. For a mean-field case (Fig. 5(a)), after $\varepsilon=0.5$ the average distance vanishes for all initial conditions taken. This means that the

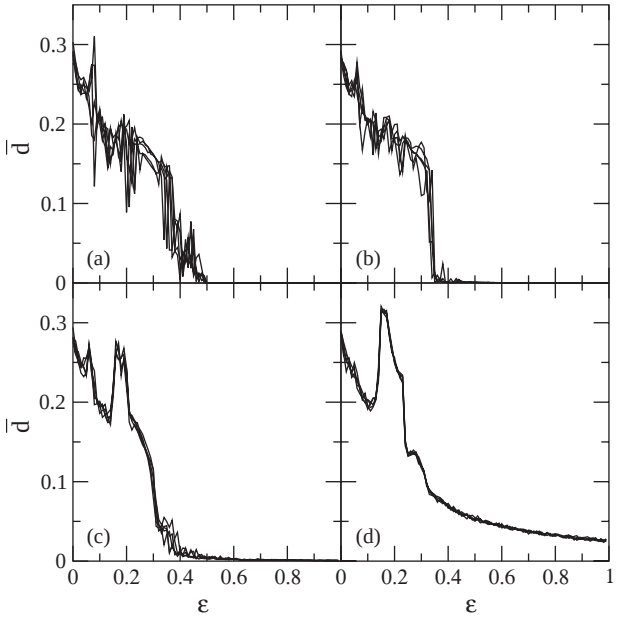

Fig. 5. Mean distance of points in the two-dimensional spatial return map with respect to the diagonal line versus the coupling strength ε for (a) $\alpha=0.0$; (b) 0.5; (c) 1.0; (d) 2.0; and at a fixed time $n=5000$.

global lattice completely synchronizes (with chaotic dynamics) for $\varepsilon > 0.5$, a fact already expected from the analysis of the corresponding Lyapunov spectrum [38,41].

When the coupling is global but not of the mean-field type (Fig. 5(b)) the average distance also tends to zero for large ε, but the threshold to chaotic synchronization is no longer at $\varepsilon = 0.5$. In fact it occurs for a larger value, indicating that it becomes increasingly difficult to synchronize the lattice as the coupling tends to be local, what is confirmed by Figs. 5(c) and (d), for which α is further increased.

A similar conclusion can be drawn on analyzing the results depicted in Fig. 6, where the average distance $\bar{d}_n$ is plotted as a function of α, for different coupling strengths. For small ε it turns out that $\bar{d}_n$ does not vary appreciably with the effective coupling range, indicating that the coupled maps will not synchronize at all. On the other hand, with stronger coupling the situation is different, since for small α (global coupling) we have small (and nearly zero) values of $\bar{d}_n$, confirming the possibility of chaotic synchronization. If the coupling is local, however, we return to the previous situation. Hence, global-type couplings favor synchronization, whereas local-type couplings do not. Strictly speaking, the fact that $\bar{d}_n = 0$ does not necessarily imply complete synchronization, either periodic or chaotic, since there could exist particular (and rare) lattice patterns for which $\bar{d}_n = 0$ without equality of $x_n^{(i)}$ (we can think of, for example, a perfect sine-wave lattice pattern).

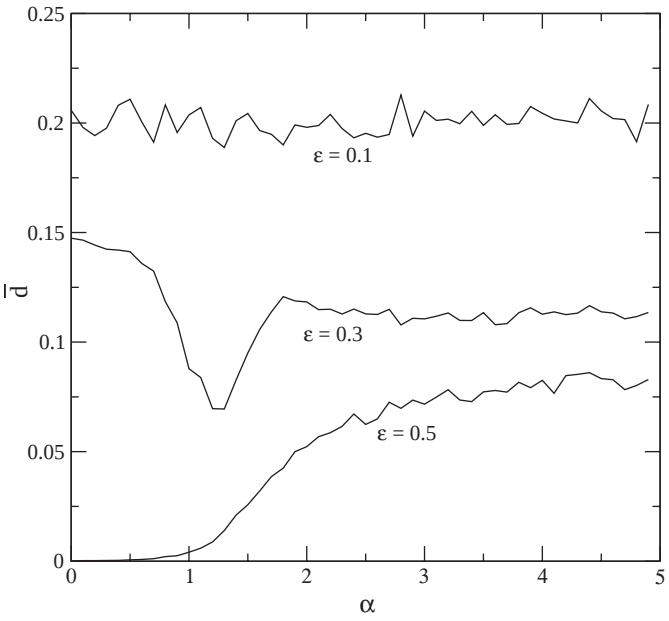

Fig. 6. Mean distance of points in the spatial return map with respect to the diagonal line versus the coupling range α for different values of ε, with $N = 1001$ maps at a fixed time $n = 5000$.

Another diagnostic of synchronization of the coupled maps is furnished by the so-called *order parameter*, introduced by Kuramoto [18,39,40]

$$z_n = R_n \exp(2\pi i \varphi_n) \equiv \frac{1}{N} \sum_{j=1}^{N} \exp(2\pi i x_n^{(j)}) \,, \tag{12}$$

where R_n and φ_n are the amplitude and angle, respectively, of a centroid phase vector for a one-dimensional lattice with periodic boundary conditions. Completely synchronized maps are such that the centroid vector is the coherent sum of all phase vectors, giving $R_n = 1$. Uncoupled maps, on the other hand, are not expected to exhibit synchronization, showing instead a pattern in which the site amplitudes $x_n^{(j)}$ are so spatially uncorrelated that they may be considered essentially as random variables. In this case the order parameter $z_n = \langle e^{2\pi i x_n^{(j)}} \rangle_j$ nearly vanishes for all times.

Fig. 7 shows the values of the order parameter magnitude at a fixed time ($n = 5000$) as a function of the coupling parameters, the strength and range. Let us first consider the case of global mean-field coupling ($\alpha = 0$). For strong coupling ($\varepsilon \gtrsim 0.5$) the order parameter is close enough to unity to ensure that synchronization of chaotic motion is achieved by the lattice as a whole. Hence, although undergoing temporally irregular dynamics, there is a very strong spatial correlation of the maps. The fact that the maps lose synchronization for ε less than 0.5 has been observed for other chaotic maps, and it can be even theoretically predicted for the special case of piecewise linear maps [38]. In Fig. 7 this transition amounts to the sharp decrease of the order parameter magnitude when $\varepsilon \lesssim 0.5$. Moreover, this result can also be inferred from the mean distance to the diagonal line in the return plot (see Fig. 5).

The transition from chaotic synchronization (spatial order with temporal chaos) to non-synchronized states with positive KS-entropy (spatial and temporal disorder) also occurs for higher values of the effective range α, but the interval for which synchronization occurs decreases with α. For a critical range $\alpha = \alpha_c \approx 0.67$ we

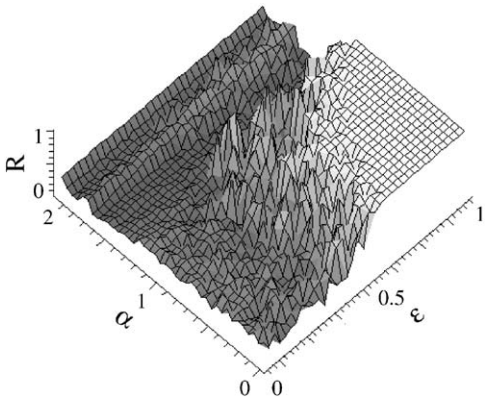

Fig. 7. Order parameter magnitude at time $n = 5000$ versus coupling strength and range, for a logistic map lattice with $N = 1001$ sites.

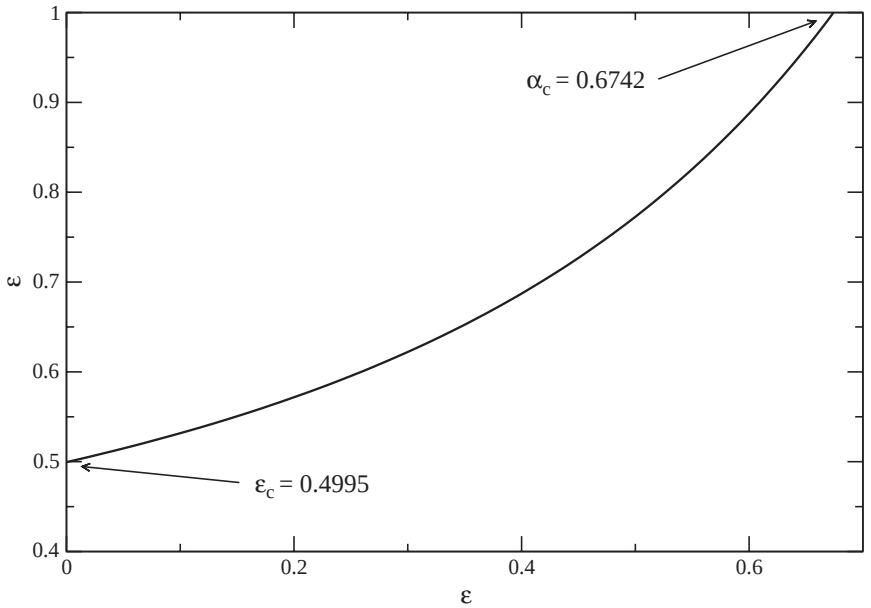

Fig. 8. Boundary between the regions of chaotic synchronization and non-synchronization in the order parameter magnitude plot of Fig. 7, as computed from Eq. (13), for $N = 1001$ maps.

cannot observe synchronization within the range $0<\varepsilon<1$. This means that, as the lattice coupling becomes more of a local nature, i.e., when the interactions are mainly with the nearest neighbors, the diffusive effect of coupling is not capable to overcome the intrinsic tendency to spatial disorder.

The boundary between synchronized ($\bar{R} = 1$) and non-synchronized ($\bar{R} \neq 1$) regions will be represented in the coupling parameter plane (ε versus α) by a curve $\varepsilon_c(\alpha)$. This curve can already be inferred from the numerical results of Fig. 7, but it can also be determined, as shown in Fig. 8, by using analytical methods, as [41]

$$\varepsilon_c(\alpha) = (1 - \mathrm{e}^{-\lambda_U})\left[1 - \frac{2}{\eta(\alpha)} \sum_{m=1}^{N'} \frac{1}{m^{\alpha}} \cos\left(\frac{2\pi m}{N}\right)\right]^{-1} \tag{13}$$

which has been derived from the Lyapunov spectrum known for completely synchronized regimes of a coupled map lattice of form (1). The intersection points between this curve and the axes are $\varepsilon_c(\alpha = 0) = 0.4995$, which denotes the critical coupling strength for the global mean-field case; and $\alpha_c = 0.6742$, which is the critical coupling range for the limit case $\varepsilon_{max} = 1.0$, such that $\varepsilon_c(\alpha_c) = \varepsilon_{max}$ [42]. These values actually depend on the lattice size, and analytical expressions for the limit ($N \to \infty$) are also available [41]. We have also considered values of ε greater than unity, for which novel phenomena are observed, like a new transition to non-synchronized

behavior for ε very large. This indicates that, for strong coupling the synchronized state may become unstable and ceases to be observed (see Refs. [41,43]).

5. Spatial correlation integral

The results obtained from the average distance to the diagonal line represent only a partial description of the spatial dynamics of the coupled map lattice, since $\bar{d}_n$ is not very sensitive to the details of the point cloud in the spatial return plot. A finer analysis requires knowing higher moments of the point cloud density in the spatial return plot. In analogy with what is done in temporal dynamics, where we investigate moments of the ergodic natural measure, we can obtain a better characterization of the point cloud density by considering the pointwise correlation of the points in the spatial return plot.

Given a spatial embedding, obtained with the delay coordinates (8), a convenient object to construct is the spatial correlation "integral", which is actually a summation over all pairs of points in the spatial return plot (at a fixed time n) and whose mutual pointwise distances are less than a certain radius ℓ [22]:

$$C_n(\ell) = \lim_{N\to\infty} \frac{1}{N^2} \sum_{i=1}^{N} \sum_{j=1}^{N} \theta(\ell - ||\xi_n^{(j)} - \xi_n^{(i)}||)\,, \tag{14}$$

where $\theta(\cdot)$ is the Heaviside unit step function, and $||\cdots||$ is a distance in the reconstructed space with a suitable metric. It suffices to use, in a R^D space, an Euclidean metric.

Roughly speaking, the correlation integral measures how concentrated are the cloud points in the spatial return plot, and no longer restricted to the vicinity of the diagonal line. Hence $C_n(\ell)$ is not just a numerical diagnostic of synchronization, but also of spatial coherence of the coupled maps. Given a preliminary indication of chaotic synchronization (like that furnished by the average distance to the diagonal line), the correlation integral would then measure how far we are from the completely synchronized case (for which the cloud would shrink to a single point). In the latter case, the correlation integral tends to the unity. On the other hand, a cloud of points uniformly scattered in the spatial return plot would give a value close to zero for $C_n(\ell)$.

The left panel of Fig. 9 shows the dependence of the spatial correlation integral with the correlation radius ℓ, for three different initial patterns of the coupled map lattice $x_0^{(i)}$. As a general trend, we observe that the correlation integral increases with ℓ monotonically for the different initial conditions used, with minor variations, from zero (when the correlation radius vanishes) to unity (for radii large enough to encompass the whole return plot). The differences between the initial conditions are best understood by considering the time evolution of the distance to the synchronization manifold D_n^2, as given by Eq. (10), and depicted for each case in the right panels of Fig. 9. At time $n = 1506$, where the correlation integral was evaluated, each initial condition yields a distance d with a slightly different value,

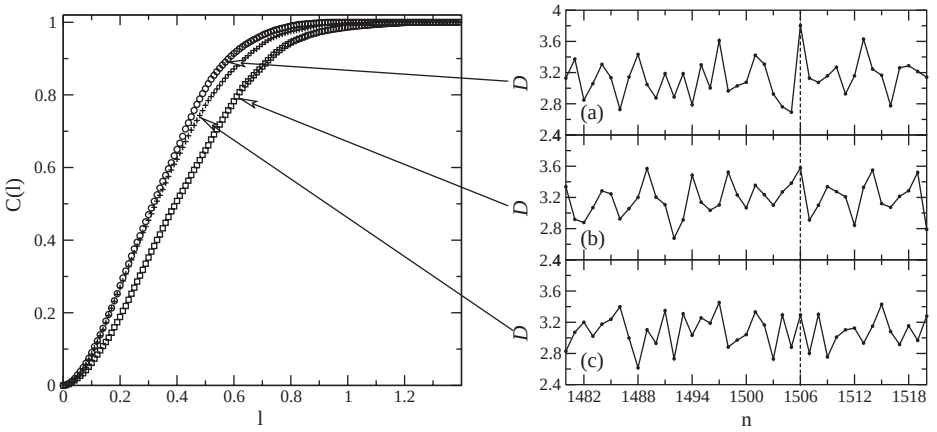

Fig. 9. Left: spatial correlation integral versus correlation radius ℓ in the spatial return plot of a lattice with $N = 201$ maps, where $\alpha = 3.735594$, $\varepsilon = 1.0$, and a fixed time $n = 1506$, for three different initial conditions. Right: time series of the distance D_n^2 to the synchronization manifold, for the initial conditions represented as circles (a), squares (b), and crosses (c).

which is reflected in the observed small deviations shown by the correlation integral (left panel of Fig. 9).

The effect of varying the coupling range, for a given strength $\varepsilon = 1.0$ is illustrated by Figs. 10(a)–(f). Each panel presents various curves corresponding to different random initial conditions. For weakly coupled maps (Fig. 10(a)) the correlation is null for small radius and increases monotonically with larger radius until it reaches its maximum value at $\ell \approx 1.0$. This is consistent with the fact that the point cloud is so uniformly scattered that the only way to get more correlation is to use larger correlation radius so as to cover the whole cloud. Even for more correlated patterns this continues to occur but for a slightly less radius. For example, when the maps are weakly coupled (Fig. 10(b)) the correlation starts to saturate after 0.9. As the coupling strength increases (Figs. 10(c)–(f)) we see that, while the curves reach unity at roughly the same value, there are realizations of the lattice (obtained from different random initial patterns) for which this saturation occurs earlier. The reason for this behavior is illustrated in Fig. 9. This fact also reflects a more pronounced tendency to point clustering when the coupling increases and, as our previous results have indicated, also to a more synchronized chaotic state.

We observed that, for small radius, the correlation integral nearly satisfies a power-law scaling, but rapidly (faster than a power-law) saturates for higher radius as already discussed. The slope of this power-law curve could be interpreted as a spatial analogue of a correlation dimension [22]. However, this is not likely to be a good measure of spatial correlation since this slope is found to increase with the embedding dimension, unlike a "real" correlation dimension, and apparently goes to infinity for very large embedding dimension.

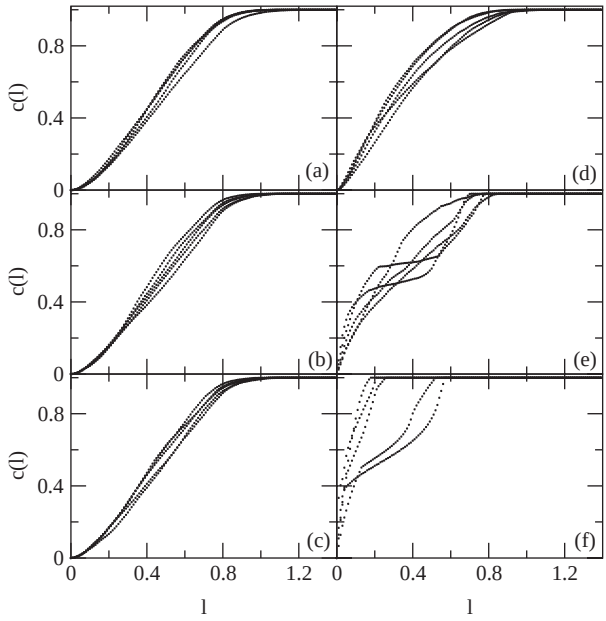

Fig. 10. Spatial correlation integral for the following (α, ε) values in the coupling parameter space: (a) $(2.0, 0.1)$; (b) $(1.0, 0.1)$; (c) $(0.5, 0.1)$; (d) $(2.0, 0.5)$; (e) $(1.0, 0.5)$; (f) $(0.5, 0.5)$. We used $N = 201$ maps at a fixed time $n = 2000$.

6. Conclusions

In this work we used a number of numerical diagnostics of spatial randomness to quantify the spatial disorder and its relation with temporal chaos, for a coupled map lattice with variable range coupling. The coupling prescription we have used depends on two key parameters: the coupling strength and range. The latter parameter can be continuous swept over a range such that our coupling varies from a global (mean-field) to a local (nearest-neighbor) one. The main tool is the spatial embedding in the form of a spatial return plot, computed at a fixed time. Synchronized and near-synchronized states can be characterized by analyzing the properties of the point cloud in such plots with respect to the diagonal line. Moreover, we quantify the clustering of points by introducing a spatial correlation integral similar to the quantity already existing for temporal dynamics.

The analyses using spatial correlation integral complement those performed using the order parameter, which is more commonly used to characterize synchronization. The correlation integral, on the other hand, is also capable to evidence collective behavior along the lattice, not necessarily related to synchronized states. Our results point that, for strong coupling and small-range parameter (global coupling) there is a pronounced tendency to synchronization of chaos in the logistic map lattice. For weaker coupling and/or larger range parameter, this synchronized state begins to

breakup in an intermittent fashion until we achieve a completely non-synchronized behavior for local coupling (effectively between nearest neighbors), even if large coupling strengths are used. This transition is characterized by non-synchronized states, but which still have some degree of spatial correlation.

The rationale for explaining this spatial behavior, with respect to variations on the coupling parameters, is the competition between the intrinsic disorder caused by the randomness of the spatio-temporal dynamics, and the diffusion effect produced by the coupling. When the latter overcomes the former, we can have synchronized behavior, even though the maps are chaotic. This occurs in the global coupling cases, where the interactions among maps are widely distributed over the lattice. In the limit, each map is coupled with the mean-field of all other maps, and diffusion in this case is greatly enhanced. Non-synchronized states result from coupling not strong enough, what occurs either if the interaction is local, or too weak to overcome spatio-temporal randomness.

Acknowledgements

This work was made possible by partial financial support from the following Brazilian government agencies: CNPq and CAPES.

References

[1] E. Fermi, J. Pasta, S. Ulam, Studies in Nonlinear Problems, I. Los Alamos report LA 1940, 1955. Reproduced in: A.C. Newell (Ed.), Nonlinear Wave Motion, American Mathematical Society, Providence, RI, 1974.
[2] A. Turing, Philos. Trans. R. Soc. London B 237 (1952) 37.
[3] G. Nicolis, I. Prigogine, Self-organization in Nonequilibrium Systems. From Dissipative Structures to Order through Fluctuations, Wiley, New York, 1977.
[4] K. Kaneko (Ed.), Theory and Applications of Coupled Map Lattices, Wiley, Chichester, 1993.
[5] U. Frisch, Turbulence, Cambridge University Press, Cambridge, 1995.
[6] T. Bohr, D.A. Rand, Physica D 52 (1991) 532.
[7] H. Chaté, P. Manneville, Physica D 32 (1988) 409.
[8] J. Brindley, K. Kaneko, T. Kapitaniak, Chaos, Solit. Fract. 4 (1994) 1193.
[9] R.R. Rosa, A.S. Sharma, J.A. Valdivia, Physica A 257 (1998) 509.
[10] F.M. Ramos, R.R. Rosa, C. Rodrigues Neto, A. Zanandrea, Physica A 283 (2000) 171.
[11] H. Nozawa, Chaos 2 (1992) 377;
S. Ishii, M. Sato, Physica D 121 (1998) 344.
[12] S. Raghavachari, J.A. Glazier, Phys. Rev. Lett. 74 (1995) 3297.
[13] P.M. Gade, C.-K. Hu, Phys. Rev. E 60 (1999) 4966.
[14] Y. Kuramoto, H. Nakao, Physica D 103 (1997) 294.
[15] Y. Kuramoto, D. Battogtokh, H. Nakao, Phys. Rev. Lett. 81 (1998) 3543.
[16] J.L. Rogers, L.T. Wille, Phys. Rev. E 54 (1996) R2193.
[17] R.L. Viana, A.M. Batista, Chaos, Solit. Fract. 9 (1998) 1931.
[18] S.E. de S. Pinto, R.L. Viana, Phys. Rev. E 61 (2000) 5154.
[19] S.E. de Souza Pinto, R.L. Viana, S.R. Lopes, Physica A 303 (2002) 339.
[20] H. Kantz, T. Schreiber, Nonlinear Time Series Analysis, Cambridge University Press, Cambridge, 1997.

[21] A. Pikovsky, M. Rosenblum, J. Kurths, Synchronization: A Universal Concept in Non-linear Sciences, Cambridge University Press, Cambridge, 2001.
[22] P. Grassberger, I. Procaccia, Physica D 9 (1983) 189.
[23] G. Paladin, A. Vulpiani, J. Phys. A 25 (1994) 4511.
[24] A. Torcini, S. Lepri, Phys. Rev. E 55 (1997) R3805.
[25] J.P. Crutchfield, K. Kaneko, in: Hao Bai Lin (Ed.), Directions in Chaos, Vol. 1, World Scientific, Singapore, 1987.
[26] K. Kaneko, Physica D 23 (1986) 436.
[27] K. Kaneko, Physica D 34 (1989) 1.
[28] K. Kaneko, Physica D 41 (1990) 137.
[29] Y.B. Pesin, Russian Math. Surveys 32 (1977) 55.
[30] D. Ruelle, Bol. Soc. Brasil Mat. 9 (1978) 83.
[31] L.A. Bunimovich, Ya.G. Sinai, Nonlinearity 1 (1988) 491.
[32] T. Gilbert, Study of Spatio-Temporal Chaos in Coupled Map Lattices, Ph.D. Thesis, Université Catholique de Louvain, 1994.
[33] M. Jiang, Y.B. Pesin, Commun. Math. Phys. 193 (1998) 675.
[34] J. Bricmont, A. Kupiainen, Physica D 103 (1997) 18.
[35] A.M. Batista, S.E. de S. Pinto, R.L. Viana, S.R. Lopes, Phys. Rev. E 65 (2002) 056209.
[36] J.M. Houlrik, M.H. Jensen, Phys. Lett. A 163 (1992) 275.
[37] K. Kaneko, Collapse of Tori and Genesis of Chaos in Dissipative Systems, World Scientific, Singapore, 1986.
[38] A.M. Batista, R.L. Viana, Physica A 308 (2002) 125.
[39] Y. Kuramoto, Chemical Oscillations, Waves, and Turbulence, Springer, Berlin, 1984.
[40] H. Sakaguchi, S. Shinomoto, Y. Kuramoto, Prog. Theor. Phys. 77 (1987) 1005.
[41] C. Anteneodo, S.E.S. Pinto, A.M. Batista, R.L. Viana, Phys. Rev. E 68 (2003) 0425202(R); Erratum: 69 (2004) 045202(E).
[42] R.L. Viana, C. Grebogi, S.E. de S. Pinto, S.R. Lopes, A.M. Batista, J. Kurths, Phys. Rev. E 68 (2003) 067204.
[43] C. Anteneodo, A.M. Batista, R.L. Viana, Phys. Lett. A 326 (2004) 227.